Multifunctional $MgFe_2O_4$/GNPs nanocomposite: Graphene-promoted visible light driven photocatalytic activity and electrochemical performance of $MgFe_2O_4$ nanoparticles

M. Israr[a,b], Javed Iqbal[a,*], Aqsa Arshad[c], P. Gómez-Romero[b], R. Benages[b]

[a] LNT, Department of Physics, Quaid-i-Azam University, Islamabad, Pakistan

[b] Catalan Institute of Nanoscience and Nanotechnology, Autonomous University of Barcelona, Spain

[c] Department of Physics, International Islamic University, Islamabad, Pakistan

*Corresponding author: javed.saggu@qau.edu.pk

Abstract

Herein, the electrochemical and photodegradation properties of magnesium ferrite and graphene-nanoplatelets nanocomposites, $(MFO)_{1-x}(GNPs)_x$, (x = 0.25, 0.50, 0.75) are reported. Benefitting from the effective interfacial interaction of the bi-phase nanocomposite and superior electrical conduction of GNPs, a significant enhancement in supercapacitive performance has been demonstrated. Interestingly, the electrochemical properties of nanocomposite electrode were found to depend on the loading ratio of GNPs. Notably the $(MFO)_{0.50}(GNPs)_{0.50}$ (50 wt. % GNPs) showed an outstanding energy storage capacity of 612 F g^{-1} at 0.5 Ag^{-1} with 21.25 Wh kg^{-1} energy density at power density of 125 W kg^{-1} and retains ~76.8% of the first cycle capacitance after continuous 1500 charge/discharge cycles. Furthermore, the $(MFO)_{0.75}(GNPs)_{0.25}$ (25 wt. % GNPs) composite demonstrates admirable photodegradation efficiency (99.3% in 60 min of visible light illumination) which is 3.2 times than that of neat MFO nanoparticles. The superior electrochemical and photodegradation performance suggest that the prepared nanocomposites can be effectively utilized in high-performance energy storage devices and low cost, eco-friendly water purification systems.

Keywords: Graphene nanoplatelets; Electrochemical capacitors; Nanocomposites; Electrode material

1. Introduction

Ecological contamination and energy crisis are currently major global concerns, because of their adverse effects [1-6]. Such issues can be resolved by developing sustainable methods for the storage of energy and wastewater treatment [7-9]. Among various energy storage technologies, supercapacitors and batteries show great potential [10, 11]. Especially supercapacitors are among the optimal choices in available systems that are used for storage of energy, because of their fast charging/discharging, ultrahigh power density and tremendous cycling stability as compared to batteries and dielectric capacitors [12-15]. However, the main problem that hinders their commercialization is their low energy density and high production cost [9, 16, 17]. Recently, a range of transition metal oxides such as $NiFe_2O_4$, $ZnCo_2O_4$, $CoFe_2O_4$ etc. have been considered as efficient materials for supercapacitor electrodes, because of their rich redox reactions and relatively low electron transfer activation energy [18-20]. Among metal oxides, ferrites consist of highly electrochemically active Fe_2O_3 component, which enables them to offer large energy storage capacity and high energy density [21-25]. However redox reactions are relatively slow in electrodes made up of metal ferrites, due to their poor conductivity. It negatively affects their supercapacitance and rate capability [25]. Furthermore ferrite nanostructures tend to aggregate during charge/discharge cycles, which bring volume changes leading to poor cycling stability [26]. These issues can be astounded by combining ferrites with highly conductive carbon derived materials e.g., carbon nano-fibers [27], carbon nanotubes [28], and graphene [29] etc.

Water contamination is another major environmental issue due to release of industrial wastewater streams containing toxic pollutants e.g. organic dyes and heavy metal ions etc. into main water bodies [30]. Elimination of these contaminants from wastewater by using suitable purification methods is imperative to wellbeing of human and aquatic life, by ensuring sustainable provision of clean drinking water. In recent years, besides the traditional water purification processes, novel techniques such as electrochemical and advance oxidation processes have been developed and utilized successfully [31]. Additionally combination of traditional water purification methods with advance oxidation processes have also been adapted effectively e.g., membrane filtration technology integrated with photocatalysis etc. [32]. Among these methods, utilization of heterogeneous photocatalysis has great benefits, including eco-friendliness, suitable operating temperatures and capability of degrading pollutants completely

without generating harmful by-products [33]. In heterogeneous photocatalysis, the light absorbed by the semiconductor excites electrons from the valence band to the conduction band resulting in generation of electrons/holes pairs. These excited electrons reduces oxygen molecules and produce super-oxide anion radicals. While the holes can also form $HO^{\bullet}$, hydroxyl radicals. These radicals called reactive oxygen species attack on the molecules of organic pollutant and decomposes them to CO_2 and H_2O as final products [34].

Transition metal ferrite have been extensively researched as photocatalysts, because of their easy magnetic separation, biocompatibility and cost-effectiveness [35]. Among ferrites, nano-phase $MgFe_2O_4$ has been recognized as efficient photo-degrading material to photodegrade organic contaminants due to its fascinating physico-chemical characteristics such as resistance to photo-corrosion and suitable band gap [36-40]. However, nano-phase $MgFe_2O_4$ is mostly semiconducting to insulating and has magnetic agglomeration, which prevents its practical application as a photocatalyst [41]. To overcome this issue, integration of $MgFe_2O_4$ nanoparticles with highly conducting graphene would be a viable option. Graphene is known to have good conducting properties and when integrated with $MgFe_2O_4$ nanoparticles, works as an electron acceptor, which can possibly lead to enhanced photocatalytic activity [42]. Furthermore, graphene sheets improve the dispersion of $MgFe_2O_4$ nanoparticles [43], which is also beneficial for the improvement of photodegradation performance of the photocatalyst.

In the present study, we investigate the electrochemical and photodegradation efficiency of $(MFO)_{1-x}(GNPs)_x$ nanocomposites fabricated by CTAB assisted, in-situ co-precipitation method. The unique structure resulting from the combination of MFO nanoparticles and GNPs in the $(MFO)_{1-x}(GNPs)_x$ nanocomposite plays effective role in augmenting their supercapacitive energy storage, and significantly enhances the dye removal efficiency. The details are given in the following sections.

2. Experimental Techniques

2.1. Preparation of $(MFO)_{1-x}(GNPs)_x$ Nanocomposites

Synthesis of $(MFO)_{1-x}(GNPs)_x$ nanocomposites have been carried out by in-situ co-precipitation method assisted by cetyl trimethylammonium bromide (CTAB) as given in Fig. 1. Following procedure was adapted to prepare nanocomposite with 25% GNPs.

300 mg graphene was dispersed in an aqueous solution consisting of 0.1 g CTAB and 6M NaOH using ultrasonic bath. Afterwards, the solution was heated to 80°C and mixed aqueous solution of $Fe(NO_3)_3 \cdot 9H_2O$ (80mM) and $Mg(NO_3)_2 \cdot 6H_2O$ (40mM) was added drop wise to it, under continuous stirring. After the reaction, (2 hours), the solid product was obtained, that was further collected and washed, using de-ionized water and ethanol respectively. The drying of the sample was performed at 60°C overnight. The obtained nanocomposite was grinded and annealed at 350°C in N_2 atmosphere for 5 h [44].

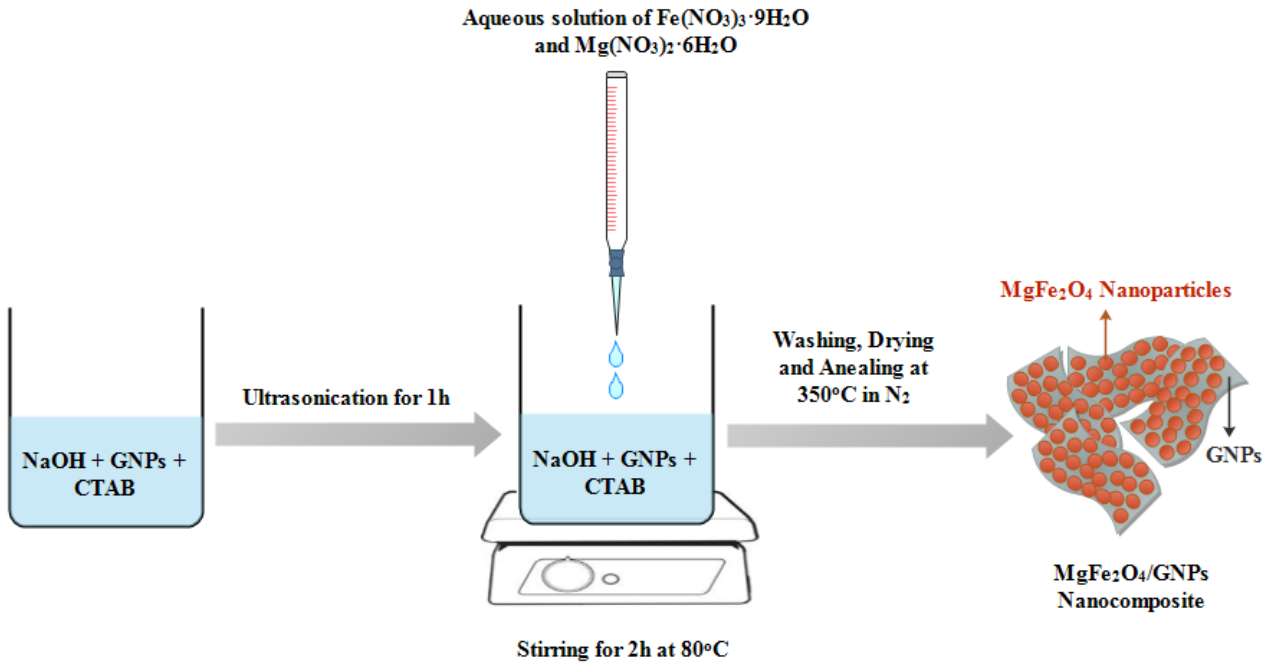

Fig. 1: Synthesis of $(MFO)_{1-x}(GNPs)_x$ nanocomposites

2.2. General Characterizations

X-ray diffractometry of the prepared samples was acquired using Malvern PANalytical system using Cu K_α (λ = 1.5406 Å) radiation source. Morphology of samples was characterized by TEM (Thermo Fisher). Room temperature XPS results were collected with XPS spectrometer (SPECS GmbH, Germany). Vibrational studies were performed using FTIR instrument (Bruker). UV–visible spectrometer (Shimadzu Co., Japan) was used to investigate the optical properties.

2.3. Supercapacitance measurements

The working electrodes were fabricated by forming mixture of the active material (80 wt. %), polyvinylidene fluoride (10 wt. %) and carbon Super P (10 wt. %) in N-methyl-2-pyrrolidinone (NMP) to form a homogeneous slurry. The obtained slurry was then deposited on Al sheet current collector through doctor blade technique followed by vacuum drying at 80°C, overnight. Two electrode symmetric Swagelok cells were assembled using glass microfiber as separator and 0.5 M K_2SO_4 as electrolyte. Biologic VMP3 potentiostat was used to measure electrochemical parameters.

2.4 Photocatalytic measurements

The photodegradation efficiency of $(MFO)_{1-x}(GNPs)_x$ nanocomposite samples have been assessed for organic dye, methylene blue (MB) using visible light source, xenon lamp (500 W). Typically, a 25 mg of the sample was dispersed in 10 mg/L MB aqueous solution. After establishing adsorption/desorption equilibrium for 30 minutes, 1 mL H_2O_2 was added to the solution. The mixture was then irradiated with visible light. Finally, about 4 mL aliquots from suspension were collected, at regular time intervals, centrifuged and were analyzed using a UV-vis spectrophotometer.

3. Results and discussions

3.1. Crystallography

The crystallinity and phase of MFO and $(MFO)_{1-x}(GNPs)_x$ samples have been studied using XRD and the results so obtained are presented in Fig. 2. The indexed peaks (220), (311), (222), (400), (331), (422), (511), and (440) planes in XRD patterns are well matched with the cubic spinel phase of MFO nanoparticles (JCPDS card No. 36-0398) indicating the phase purity of MFO sample [45]. It is clear from Fig. 2 that the peak corresponding GNPs' (002) plane lies at $2\theta = 26.5^{o}$ in the composite samples [46].

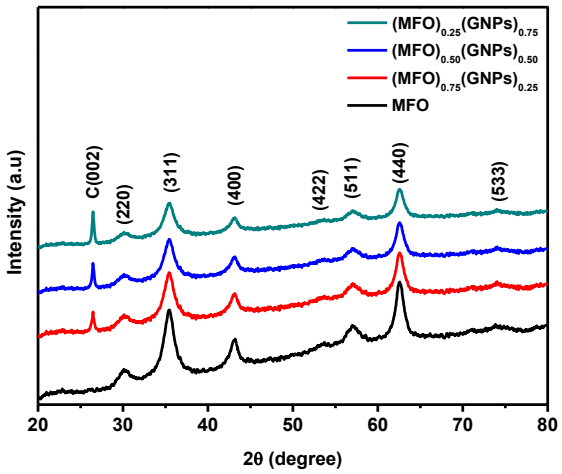

Fig. 2: X-ray diffractograms of $(MFO)_{1-x}(GNPs)_x$ materials.

3.2. TEM Analysis

Morphology of the neat MFO and the composite materials is given in Fig. 3. The TEM image of neat MFO shown in Fig. 3(a), which depicts that MFO has grown in the form of nanoparticles with sizes that range from 6 to 30 nm. The TEM images of $(MFO)_{1-x}(GNPs)_x$ in Fig. 3(b)-(d) depict that MFO nanoparticles are uniformly anchored on GNPs sheets. The results describe the successful formation of nanocomposites.

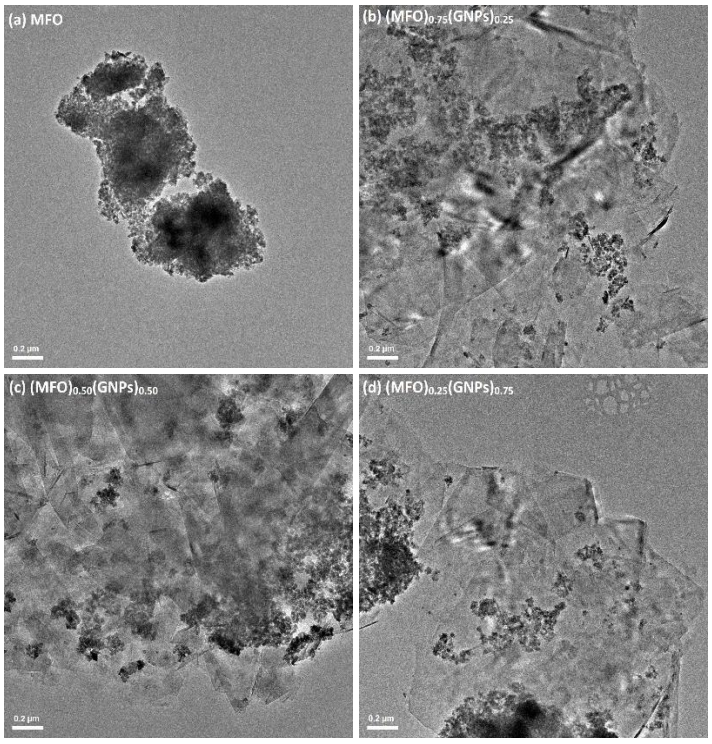

Fig. 3: TEM image of neat MFO (a), and $(MFO)_{1-x}(GNPs)_x$ nanocomposites (b)-(d).

It is notable that the density of nanoparticles on the surface of GNPs decreases with the increasing content of GNPs. The sheet like structure of GNPs favors the prevention of the MFO nanoparticles to form aggregates and enable their fine dispersion over the surface of GNPs. Whereas, MFO nanoparticles work as intercalates for GNPs and hinder their restacking. This interfacial contact helps in enhancing the contact of electrolyte ions with the active sites of the composite electrode leading to accelerated redox processes [47].

3.3. XPS Analysis

XPS investigation was carried out to inspect the detailed electronic structure and valence states of the prepared samples and the results are presented in Fig. 4.

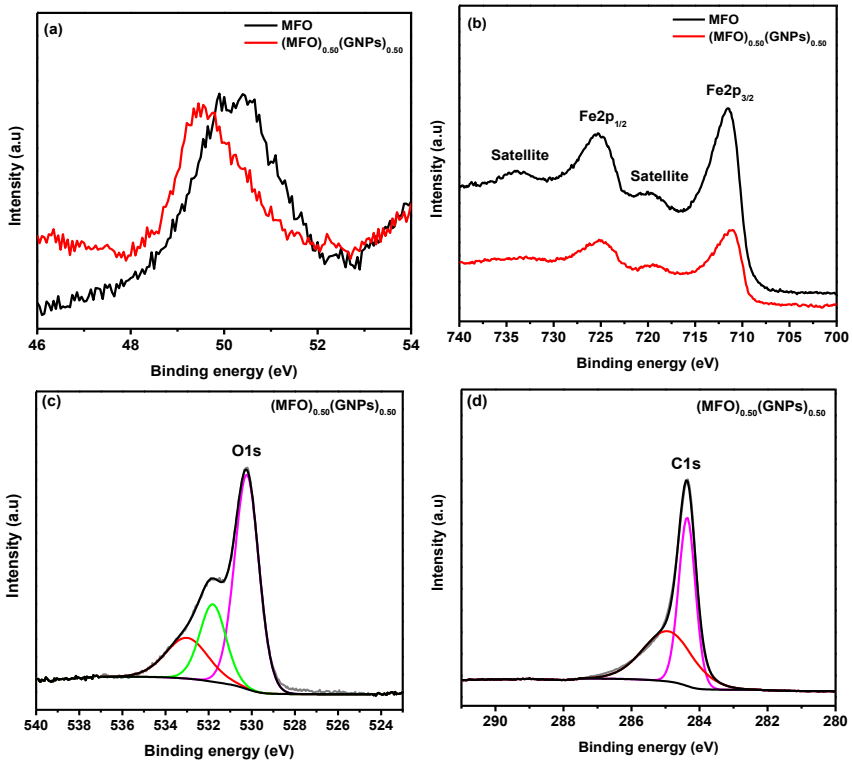

Fig. 4: High resolution XPS spectra of $(MFO)_{1-x}(GNPs)_x$ samples.

The peak at 50.18 eV (Fig. 4 (a)) is attributed to Mg^{2+} state in MFO nanoparticles [48]**.** The Fe 2p binding energy peak consists of two components Fe $2p_{1/2}$ and Fe $2p_{3/2}$ with maxima at 725.3 eV and 711.4 eV respectively as given in Fig. 4(b). The two satellite peaks at 719. 7 eV and 734 eV confirm the Fe^{+3} state [49]. The observed Fe 2p and Mg 2p photoelectron peak in

$(MFO)_{50}(GNPs)_{50}$ sample is slightly shifted towards the lower energy. This red shift in Mg 2p and Fe 2p peaks may be due to the intimate interface bondage between MFO and GNPs due to π-π interaction [50]. The wide-angle O 1s XPS photoelectron spectra of $(MFO)_{50}(GNPs)_{50}$ sample, presented in Fig. 4(c), can be resolved into three components with maxima at 530.1 eV, 531.8 eV and 533 eV. These peaks arise due to Mg-O-Mg bond, Mg–O–H and oxygen, respectively [50, 51]. The C1s spectrum exhibit two resolved peaks positioned at 284.35 eV, 285 eV shown in Fig. 4 (d), which can be ascribed to C=C and C−C covalent bonds respectively [52].

3.4. Optical properties

UV-vis spectroscopy gives useful information about optical properties of photocatalysts. The UV-vis spectra of neat MFO and $(MFO)_{1-x}(GNPs)_x$ nanocomposites have been shown in Fig. 5.

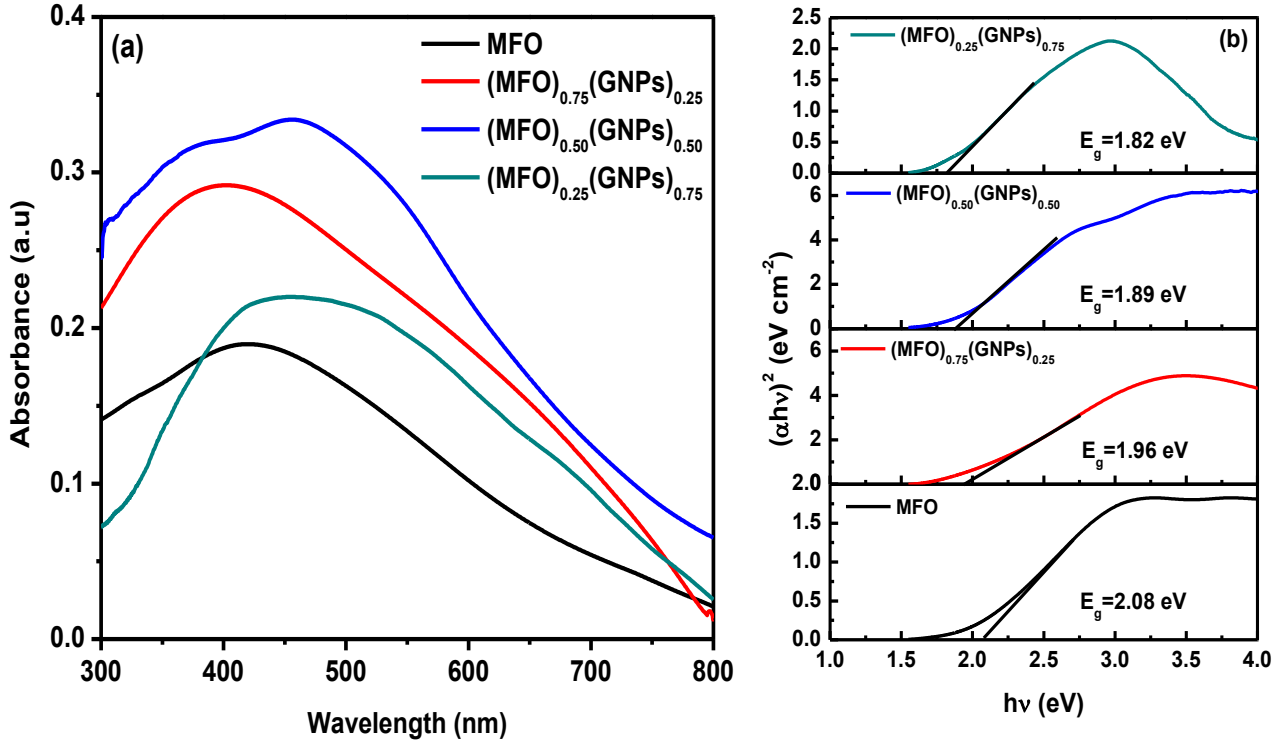

Fig. 5: (a) UV-vis spectra, (b) Tauc's plots of $(MFO)_{1-x}(GNPs)_x$ samples

Clearly absorption of $(MFO)_{1-x}(GNPs)_x$ samples shift towards more visible region with the increasing loading ratio of GNPs , which suggests that GNPs enhances the visible light absorption capability of

MFO nanoparticles. Hence, a visible light initiated photocatalytic activity of the prepared nanocomposite photocatalysts is anticipated. The bandgaps of the synthesized samples have been evaluated with the help of Tauc's equation [53], which come out to be 2.08, 1.96, 1.89 and 1.82 eV for MFO and $(MFO)_{1-x}(GNPs)_x$ nanocomposites with (x = 0, 0.25, 0.50, and 0.75) respectively. The GNPs loading ratio dependent red shift in band gap has been observed, which could possibly be due to creation of Fe–O–C bonds and formation of mid-gap energy states in MFO nanoparticles [54].

3. 5. FTIR analysis

Fig. 6 depicts the results FTIR spectroscopy of MFO and $(MFO)_{1-x}(GNPs)_x$ composite samples.

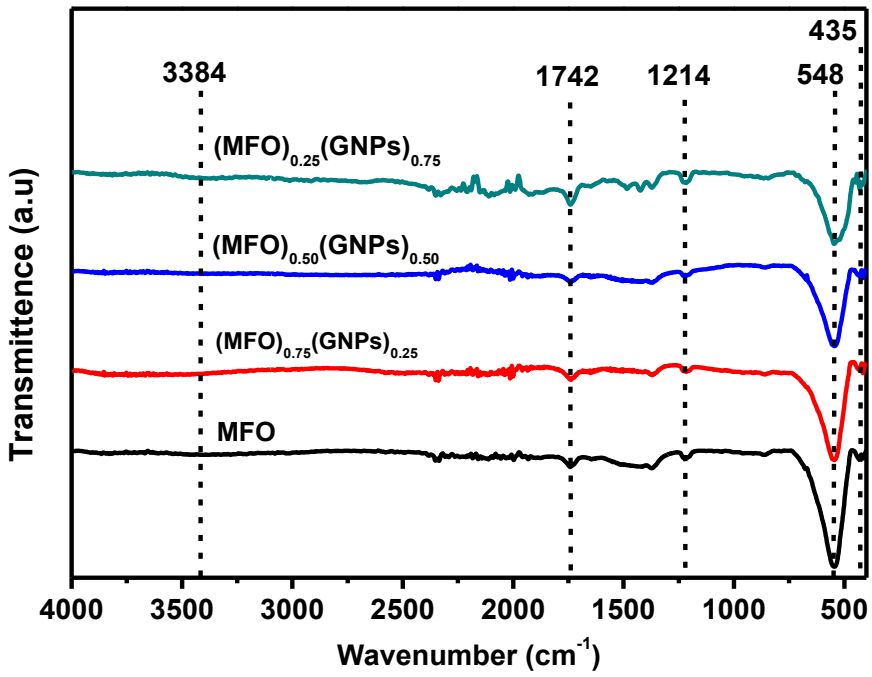

Fig. 6: FTIR spectra of neat MFO and $(MFO)_{1-x}(GNPs)_x$ nanocomposites

The bands observed at 435 $cm^{-1}$and 548 cm^{-1} are attributed to the Mg–O and Fe–O bonds stretching vibrations in MFO, confirming the successful synthesis of MFO nanoparticles [55]. Furthermore, the absorption bands at ~1214 cm^{-1} and ~1742 cm^{-1} can be ascribed to observed O−H bending vibration and the bands at ~3384 cm^{-1} originates from the hydroxyl (-OH) functional group [56, 57]. The bands in the FTIR spectrum of $(MFO)_{1-x}(GNPs)_x$ sample are slightly shifted to the lower wavenumbers suggesting strong interaction between MFO and GNPs [58].

4. Electrochemical performance

4.1. CV and GCD measurements

A comparative analysis of CV profiles obtained at 5 mVs^{-1} for MFO and $(MFO)_{1-x}(GNPs)_x$ electrodes are shown in Fig. 7(a). Clearly, the CV curve of pristine MFO and $(MFO)_{1-x}(GNPs)_x$ electrodes have quasi-rectangular shape, suggesting their good capacitive performance. Obviously, the area under the CV curve is maximum for $(MFO)_{50}(GNPs)_{50}$ is maximum as compared to the other samples, showing that the energy storage capacity of $(MFO)_{50}(GNPs)_{50}$ electrode is highest among all the prepared electrodes. This might be due to the synergistic effects arising in nanocomposites due to MFO and GNPs, both, at this optimum GNPs loading ration [59].

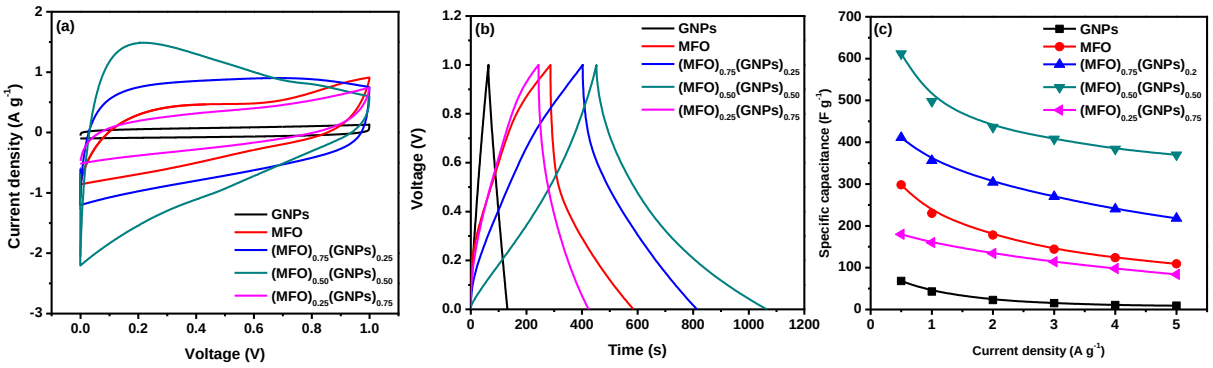

Fig. 7: (a) CV profiles at 5 mVs^{-1}, (b) GCD profiles at 0.5 Ag^{-1}, (c) specific capacitance at different current densities for $(MFO)_{1-x}(GNPs)_x$ samples

Fig.7 (b) shows the GCD profiles corresponding to MFO and $(MFO)_{1-x}(GNPs)_x$ electrodes. The slightly curved shape in the discharge profiles of all the samples, indicates the contribution of pseudocapacitance originated from redox reaction at the surface [60]. As clear from the Fig.7 (b), the Ohmic drop (IR-drop) of $(MFO)_{50}(GNPs)_{50}$ electrode is minimum among all the prepared electrodes, which suggests the fast electrochemical response, improved reversibility as well as the excellent conducting nature of the electrode [61]. The specific capacitance of a single electrode (Cs, Fg^{-1}) can be calculated using the equation [62]

$$C_s = \frac{4I\,\Delta t}{m\Delta V} = 4C_T \qquad (2)$$

Here, m is the combined mass of the nanocomposite (g), Δt is the time of discharge (s), I is the discharging current (A), ΔV symbolizes the potential window (V) and C_T represents specific capacity of the device (F g^{-1}). The specific capacitance for MFO and $(MFO)_{1-x}(GNPs)_x$ nanocomposites are evaluated to be 298, 411, 612 and 180 F g^{-1} respectively at 0.5 A g^{-1}. The admirable supercapacitance of $(MFO)_{1-x}(GNPs)_x$ electrodes might be because of the synergistic effects arising from the GNPs (double layer capacitance) and MFO (pseudocapacitance) as well as the improved distribution of MFO nanoparticles on the GNPs surface. Notably, the supercapacitance decreases drastically by increasing GNPs content to 75 wt. %. This drop in supercapacitance can be ascribed to the excessive graphene present in the sample [63, 64]. Fig. 7(c) shows the dependence of specific capacitance on current density. The $(MFO)_{50}(GNPs)_{50}$ electrode is able to provide comparatively greater specific capacitance at large current densities, suggesting its superior rate performance and fast I-V response [65].

4.2 Energy-Power density, EIS spectroscopy and cyclic stability

The energy density, E, and the power density, P, of MFO and $(MFO)_{1-x}(GNPs)_x$ electrodes are calculated using the following equations [66],

$$Energy\ density = E = \frac{0.5 C_T (\Delta V)^2}{3.6} \quad (3)$$

$$Power\ density = P = \frac{E}{\Delta t} \quad (4)$$

Here, ΔV and Δt are potential window (V) and the discharge time (h), while C_T is obtained from Equation (2). Fig. 8 (a) depicts Ragone plots for MFO and $(MFO)_{1-x}(GNPs)_x$ electrodes**,** at power density of 125 W kg^{-1}.

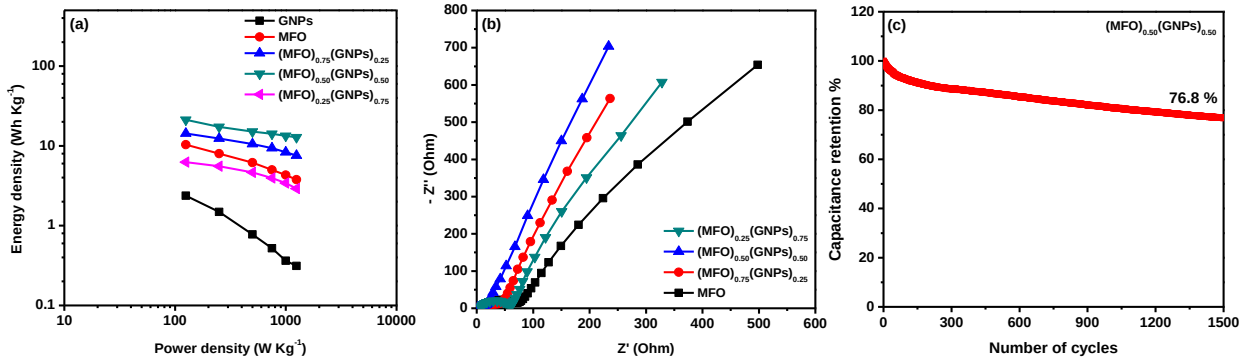

Fig. 8: (a) Ragone plots, (b) EIS spectra, (c) performance for $(MFO)_{1-x}(GNPs)_x$ electrodes

The energy density of the prepared electrodes has been calculated to be 10.3 Wh Kg^{-1}, 14.2 Wh Kg^{-1}, 21.2 Wh Kg^{-1} and 6.2 Wh Kg^{-1} respectively. The excellent energy density of $(MFO)_{50}(GNPs)_{50}$ electrode at this optimal graphene ratio might be due to the increased Faradic contribution to the specific capacitance and highly porous structure of the electrode material resulting from better dispersion of MFO nanoparticles at GNPs [67].

Nyquist curves of MFO and $(MFO)_{1-x}(GNPs)_x$ electrodes presented in Fig. 8(b), exhibit a semicircular and a linear portion. The radius of the semicircular part is attributed to the interfacial resistance between electrode and electrolyte. As clear from the Fig. 8(b) that the radius of semicircular part, in case of $(MFO)_{50}(GNPs)_{50}$ electrode, is significantly smaller than that of other prepared electrodes, indicating its minimum resistivity at the interface of electrode and electrolyte. Which may be attributed to the enhancement in the conductivity of MFO nanoparticles induced by graphene, in the nanocomposite. Furthermore, the straight-line portion of the Nyquist plot is more vertical as compared to other electrodes showing reduced diffusive resistivity of electrolyte ions in the $(MFO)_{50}(GNPs)_{50}$ electrode. The lower diffusive resistance can be ascribed to the improved porosity of the composite material [68].

The cycle stability of the $(MFO)_{50}(GNPs)_{50}$ symmetric supercapacitor has been tested for 1500 cycles of charging and discharging at 5 Ag^{-1}. Fig. 8 (c) depicts that the symmetric device retains 76.7% specific capacity relative to that of the first cycle, which indicates the brilliant cyclic permanence of the $(MFO)_{50}(GNPs)_{50}$ electrode. The high cycling stability of $(MFO)_{50}(GNPs)_{50}$ electrode is due to the synergistic improvements made by MFO nanoparticles and GNPs. This excellent cycling stability shows that the MFO nanoparticles anchored to GNPs do not experience significant volume change or decomposition during charge discharge/discharge cycles [69]. The presence of GNPs in the nanocomposite buffers the volume changes in the process.

The outstanding electrochemical efficiency of the $(MFO)_{1-x}(GNPs)_x$ electrodes is assigned to combined effects resulting from the effective attachment of component materials (i.e., MFO nanoparticles and GNPs) within the nanocomposite system. Firstly, the small-size distribution of the MFO nanoparticles grafted to the surface of GNPs provide large number of electroactive sites

for electrochemical reactions**,** which in turn contribute to enhancement of the total charge storage. Secondly, the inter-connected GNPs sheets in the nanocomposite system provide conducting pathways for the fast electron transfer, during the electrochemical reaction. Consequently, these factors greatly enhance the energy storage capacity and rate capability of the composite electrodes [70]. Moreover, the robust interfacial interaction and better dispersion of MFO nanoparticles over the surface of GNPs provide the composite electrodes an exceptional structural stability [71], which leads to improved cyclic performance.

5. Photocatalysis

The photocatalytic performance of MFO nanoparticles and the composite samples has been explored for the visible light mediated photodegradation of MB dye. Fig. 9 depicts the photocatalytic degradation of MB caused by MFO and $(MFO)_{1-x}(GNPs)_x$ nanocomposites. It has been found that within 60 min of irradiation, approximately 16% and 31% of the MB gets degraded by neat GNPs and MFO nanoparticles respectively. Higher photodegradation efficiencies i.e., 99.3%, 90.1% and 67.7% have been observed for $(MFO)_{1-x}(GNPs)_x$ (x = 0.25, 0.50, 0.75) nanocomposite photocatalysts, respectively, within the same interval of time.

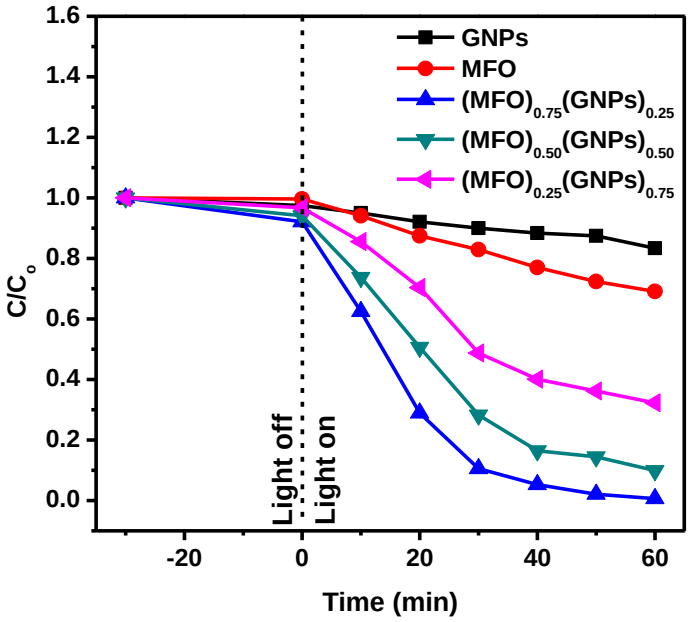

Fig. 9: (a) Photodegradation of MB by MFO, GNPs and $(MFO)_{1-x}(GNPs)_x$ nanocomposites.

The results demonstrate that incorporating GNPs with MFO nanoparticles could considerably improve the photocatalytic efficiency up to a certain optimum GNPs loading ratio and then decreases beyond that ratio. The decrease in photocatalytic activity has been observed previously

and might be because of the visible shielding produced by GNPs [72]. From the experimental results, it can be inferred that the degradation of MB dye is governed by the synergistic contribution of two possible mechanisms i.e., photocatalytic and photo-Fenton reaction as presented in Fig. 10. The photo-generated electrons and holes produce reactive oxygen species (e.g. $\bullet O_2^-$ and •OH radicals) during the photocatalytic reaction [73-75]**.** While in photo-Fenton reaction the mutual conversion of Fe^{3+}/Fe^{2+} ion pairs causes H_2O_2 in the test solution to form •OH radicals [76]. These radicals attack MB dye molecules that are adsorbed on the catalyst surface and degrade the dye to H_2O and CO_2 as final products.

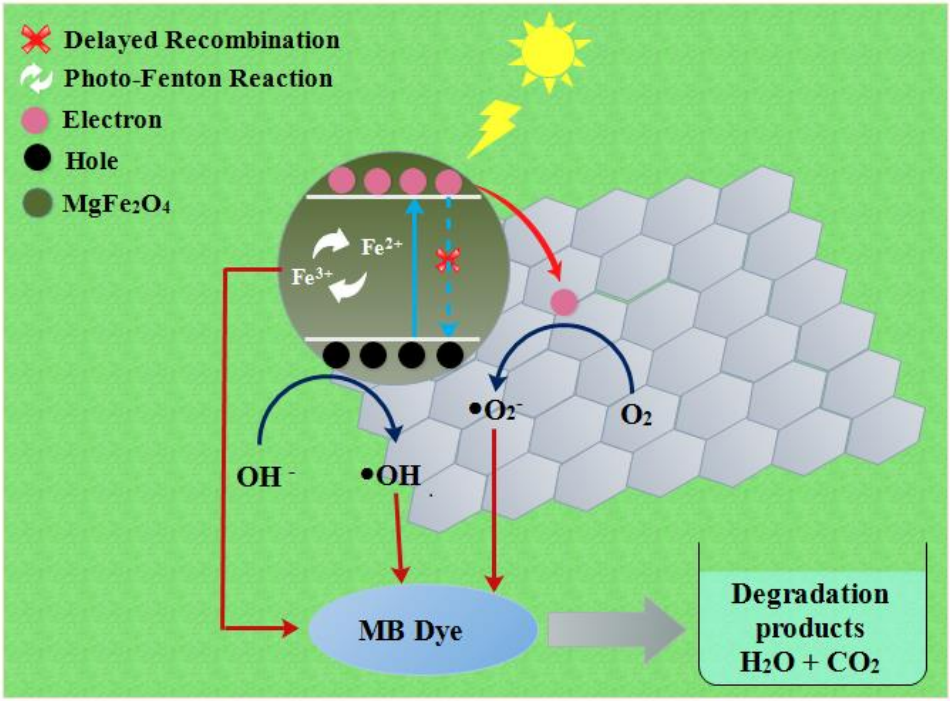

Fig. 10: Photocatalytic reaction mechanism of $(MFO)_{1-x}(GNPs)_x$ composite materials

The enhancement of photo-degradation of MB by the composite sample can be attributed to various factors such as improved charge separation efficiency, accelerated photo-Fenton reaction, and reduced agglomeration of the ferrite nanoparticles. By incorporation of GNPs in the composite system, photo-generated electrons in ferrites can be readily accepted by GNPs to reduce the charge carrier recombination. Which in turn enhances the photocatalytic activity [77]. Here, GNPs play two key roles for the enhancement of the photo-catalytic activity of the $(MFO)_{1-x}(GNPs)_x$ nanocomposites. First, as reported previously, the planar π-conjugated

structure of GNPs makes it an excellent electron accepting material [78, 79]. Therefore, electrons that are excited to the conduction band of MFO can effectively transfer to GNPs through mechanism of percolation [80]. This helps in reducing recombination of charge carriers and thus more electrons are available for the formation of reactive species as shown in Fig. 10. Consequently, enhanced photo-degradation of MB dye is favored. Second, the highly conducting nature of GNPs enables fast charge carrier transport, which helps in their effective carriers separation during photocatalytic reaction. Furthermore, MFO, present in the nanocomposite helps to increase the rate of photo-Fenton reaction, consequently, the ability of the nanocomposite to degrade MB dye is improved [81]. Lastly, the reduced agglomeration makes surface area higher to allow better adsorption of photocatalyst, which is crucial for the enhanced photo-degradation of MB.

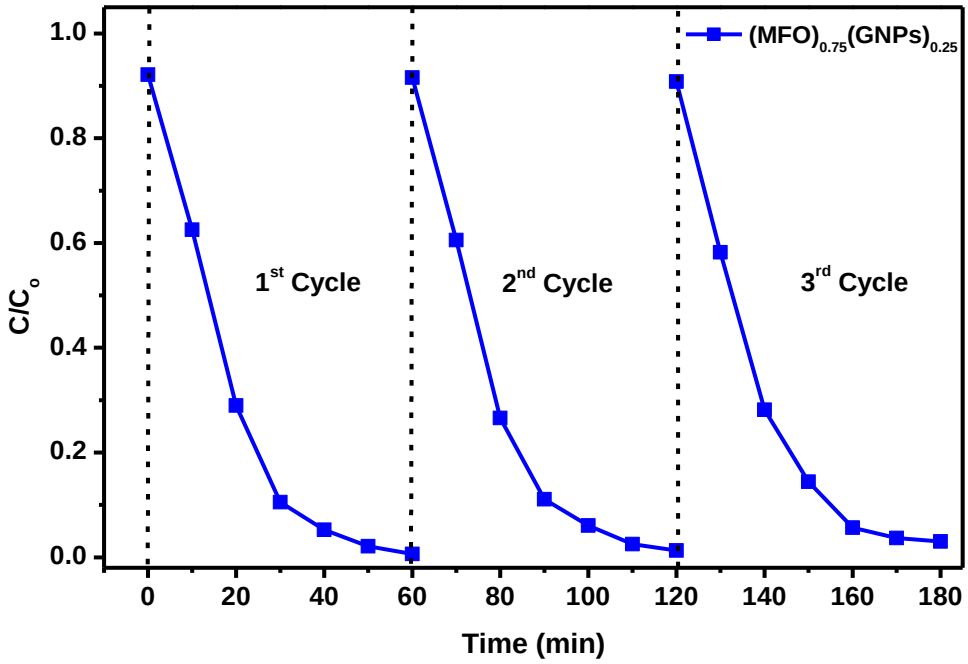

Fig. 11: Stability tests for $(MFO)_{0.75}(GNPs)_{0.25}$ composite sample

The cyclic stability of the photocatalyst is crucial factor to ensure its cost effectiveness and its suitability for commercialization. The re-usability of $(MFO)_{0.75}(GNPs)_{0.25}$ nanocomposite sample has been tested for three consecutive cycles and the results are shown in Fig. 11. It is obvious from the results that there is negligible change in the photocatalytic activity after repeated use, which indicates that the photocatalyst has outstanding cycling stability. This study

highlights the possible application of $MgFe_2O_4$/GNPs nanocomposites in effective low-cost energy storage and water purification systems, on practical grounds.

Table. 1: A comparison of the similar work done before

Photocatalysis						
Photocatalyst	**MB concentration /volume**	**Amount of photocatalyst**	**degradation time/efficiency**	**Light Source**	**Synthesis Method**	**Ref.**
$MgFe_2O_4$/rGO	250 mL of 40 ppm MG	40 mg	120 min/98%	Sunlight	sol-gel	[57]
$MgFe_2O_4$/ rGO	20 mg L^{-1}/100 mL MO	50 mg	60 min/99%	300 W	solvothermal	[82]
Dispersion and attachment to graphene not good/ No graphene ratio dependent study						
Supercapacitors						
Sample	Electrolyte	Specific capacitance (Fg^{-1})		Synthesis Method		Ref.
Zn doped $MgFe_2O_4$	1 M Na_2SO_4	484.6 at 1 $mAcm^{-2}$		sol–gel citrate method		[83]
Li storage performance of $MgFe_2O_4$/Graphene has been studied but supercapacitor performance has not been reported [84, 85]						
Combined study of $MgFe_2O_4$/Graphene for photocatalysis and supercapacitors has not been reported						

Table. 1 depicts a comparison of the same nanocomposites with the work presented here, to address the novelty. The novelty of the work is discussed and presented above.

6. Conclusion

In this work, $(MFO)_{1-x}(GNPs)_x$ nanocomposite with different GNPs loading ratio (25, 50 and 75%) are fabricated and are tested as electrode materials for symmetric supercapacitors. It is notable that $(MFO)_{0.50}(GNPs)_{0.50}$ nanocomposite has maximum specific energy storage capacity of 612 F g^{-1} and a highest energy density, 21.25 Wh Kg^{-1}. This nanocomposite electrode shows 76.7% retention for 1500 cycles of charge/discharge. Substantial enhancement in the supercapacitive performance of the composite sample mainly results due to better conductivity, improved interfacial charge transfer and structural stability. The photocatalytic activity has been found to be highest for the composite with 25% GNPs content, which can be attributed to the reduced agglomeration of MFO nanoparticles, decreased recombination of charge carriers and conducting nature of GNPs. Hence, the supercapacitor electrodes and photocatalysts based on $(MFO)_{1-x}(GNPs)_x$ nanocomposites could be potentially used in energy storage devices and water purification systems respectively.

7. Acknowledgement

The financial support of this work by the Higher Education Commission of Pakistan (HEC), NRPU (Grant No: 9640/Federal/NRPU/R&D/HEC/2017) and IRSIP (Grant No: 1-8/HEC/HRD/2017/8412 PIN: IRSIP 39 PSc 15) is gratefully appreciated.

8. References

g[1] W. Du, X. Wang, J. Zhan, X. Sun, L. Kang, F. Jiang, X. Zhang, Q. Shao, M. Dong, H. Liu, Biological cell template synthesis of nitrogen-doped porous hollow carbon spheres/MnO2 composites for high-performance asymmetric supercapacitors, Electrochimica Acta 296 (2019) 907-915.
[2] P. Zhao, M. Yao, H. Ren, N. Wang, S. Komarneni, Nanocomposites of hierarchical ultrathin MnO2 nanosheets/hollow carbon nanofibers for high-performance asymmetric supercapacitors, Applied Surface Science 463 (2019) 931-938.
[3] F. Liao, X. Han, D. Cheng, Y. Zhang, X. Han, C. Xu, H. Chen, MnO2 hierarchical microspheres assembled from porous nanoplates for high-performance supercapacitors, Ceramics International 45(1) (2019) 1058-1066.
[4] S. Wen, K. Qin, P. Liu, N. Zhao, C. Shi, L. Ma, E. Liu, Ultrafine Ni (OH) 2 nanoneedles on N-doped 3D rivet graphene film for high-performance asymmetric supercapacitor, Journal of Alloys and Compounds 783 (2019) 625-632.
[5] N. Hu, L. Huang, W. Gong, P.K. Shen, High-Performance Asymmetric Supercapacitor Based on Hierarchical NiMn2O4@ CoS Core–Shell Microspheres and Stereotaxically Constricted Graphene, ACS Sustainable Chemistry & Engineering 6(12) (2018) 16933-16940.
[6] V. Dutta, S. Sharma, P. Raizada, A. Hosseini-Bandegharaei, V.K. Gupta, P. Singh, Review on augmentation in photocatalytic activity of CoFe2O4 via heterojunction formation for photocatalysis of organic pollutants in water, Journal of Saudi Chemical Society 23(8) (2019) 1119-1136.
[7] H. Jia, Y. Cai, J. Lin, H. Liang, J. Qi, J. Cao, J. Feng, W. Fei, Heterostructural Graphene Quantum Dot/MnO2 Nanosheets toward High-Potential Window Electrodes for High-Performance Supercapacitors, Advanced Science 5(5) (2018) 1700887.
[8] S. Jadhav, R.S. Kalubarme, C. Terashima, B.B. Kale, V. Godbole, A. Fujishima, S.W. Gosavi, Manganese dioxide/reduced graphene oxide composite an electrode material for high-performance solid state supercapacitor, Electrochimica Acta 299 (2019) 34-44.
[9] W. Fan, Y. Shi, W. Gao, Z. Sun, T. Liu, Graphene–Carbon Nanotube Aerogel with a Scroll-Interconnected-Sheet Structure as an Advanced Framework for a High-Performance Asymmetric Supercapacitor Electrode, ACS Applied Nano Materials 1(9) (2018) 4435-4441.
[10] D. Jiang, H. Liang, W. Yang, Y. Liu, X. Cao, J. Zhang, C. Li, J. Liu, J.J. Gooding, Screen-printable films of graphene/CoS2/Ni3S4 composites for flexible and arbitrary-shaped all-solid-state hybrid supercapacitor device, Carbon 146 (2019) 557-567.
[11] J. Ao, R. Miao, J. Li, Flexible solid-state supercapacitor based on reduced graphene oxide-enhanced electrode materials, Journal of Alloys and Compounds 802 (2019) 355-363.
[12] J.A. Hondred, I.L. Medintz, J.C. Claussen, Enhanced electrochemical biosensor and supercapacitor with 3D porous architectured graphene via salt impregnated inkjet maskless lithography, Nanoscale Horizons 4(3) (2019) 735-746.
[13] Y. Jiao, C. Qu, B. Zhao, Z. Liang, H. Chang, S. Kumar, R. Zou, M. Liu, K.S. Walton, High-Performance Electrodes for a Hybrid Supercapacitor Derived from a Metal-Organic Framework/Graphene Composite, ACS Applied Energy Materials 2(7) (2019) 5029-5038.

[14] Y. Cheng, Y. Zhang, Q. Wang, C. Meng, Synthesis of amorphous MnSiO3/graphene oxide with excellent electrochemical performance as supercapacitor electrode, Colloids and Surfaces A: Physicochemical and Engineering Aspects 562 (2019) 93-100.
[15] Y. Wang, W. Zhang, X. Guo, K. Jin, Z. Chen, Y. Liu, L. Yin, L. Li, K. Yin, L. Sun, Ni–Co Selenide Nanosheet/3D Graphene/Nickel Foam Binder-Free Electrode for High-Performance Supercapacitor, ACS applied materials & interfaces 11(8) (2019) 7946-7953.
[16] X. Yang, H. Niu, H. Jiang, Q. Wang, F. Qu, A high energy density all-solid-state asymmetric supercapacitor based on MoS 2/graphene nanosheets and MnO 2/graphene hybrid electrodes, Journal of Materials Chemistry A 4(29) (2016) 11264-11275.
[17] H.R. Naderi, P. Norouzi, M.R. Ganjali, Electrochemical study of a novel high performance supercapacitor based on MnO2/nitrogen-doped graphene nanocomposite, Applied Surface Science 366 (2016) 552-560.
[18] J. Jiang, Y. Li, J. Liu, X. Huang, C. Yuan, X.W.D. Lou, Recent advances in metal oxide-based electrode architecture design for electrochemical energy storage, Advanced Materials 24(38) (2012) 5166-5180.
[19] X. Xu, K. Cao, Y. Wang, L. Jiao, 3D hierarchical porous ZnO/ZnCo 2 O 4 nanosheets as high-rate anode material for lithium-ion batteries, Journal of Materials Chemistry A 4(16) (2016) 6042-6047.
[20] M. Reddy, Y. Xu, V. Rajarajan, T. Ouyang, B. Chowdari, Template free facile molten synthesis and energy storage studies on MCo2O4 (M= Mg, Mn) as anode for Li-ion batteries, ACS Sustainable Chemistry & Engineering 3(12) (2015) 3035-3042.
[21] N. Sivakumar, S. Gnanakan, K. Karthikeyan, S. Amaresh, W. Yoon, G. Park, Y. Lee, Nanostructured MgFe2O4 as anode materials for lithium-ion batteries, Journal of Alloys and Compounds 509(25) (2011) 7038-7041.
[22] Y. Pan, Y. Zhang, X. Wei, C. Yuan, J. Yin, D. Cao, G. Wang, MgFe2O4 nanoparticles as anode materials for lithium-ion batteries, Electrochimica Acta 109 (2013) 89-94.
[23] H. Qiao, L. Luo, K. Chen, Y. Fei, R. Cui, Q. Wei, Electrospun synthesis and lithium storage properties of magnesium ferrite nanofibers, Electrochimica Acta 160 (2015) 43-49.
[24] C. Gong, Y.-J. Bai, Y.-X. Qi, N. Lun, J. Feng, Preparation of carbon-coated MgFe2O4 with excellent cycling and rate performance, Electrochimica Acta 90 (2013) 119-127.
[25] A.K. Rai, T.V. Thi, J. Gim, J.J.M.c. Kim, Combustion synthesis of MgFe2O4/graphene nanocomposite as a high-performance negative electrode for lithium ion batteries, Materials characterization 95 (2014) 259-265.
[26] X. Zhang, T. Chen, D. Yan, W. Qin, B. Hu, Z. Sun, L.J.E.A. Pan, MgFe2O4/reduced graphene oxide composites as high-performance anode materials for sodium ion batteries, Electrochimica Acta 180 (2015) 616-621.
[27] F. Raza, X. Ni, J. Wang, S. Liu, Z. Jiang, C. Liu, H. Chen, A. Farooq, A. Ju, Ultrathin honeycomb-like MnO2 on hollow carbon nanofiber networks as binder-free electrode for flexible symmetric all-solid-state supercapacitors, Journal of Energy Storage 30 (2020) 101467.
[28] S.S. Raut, B.R. Sankapal, M.S.A. Hossain, S. Pradhan, R.R. Salunkhe, Y. Yamauchi, Zinc ferrite anchored multiwalled carbon nanotubes for high-performance supercapacitor applications, European Journal of Inorganic Chemistry 2018(2) (2018) 137-142.
[29] L.H. Nonaka, T.S. Almeida, C.B. Aquino, S.H. Domingues, R. V. Salvatierra, V.H. Souza, Crumpled Graphene Decorated with Manganese Ferrite Nanoparticles for Hydrogen Peroxide Sensing and Electrochemical Supercapacitors, ACS Applied Nano Materials 3(5) (2020) 4859-4869.
[30] P. Singh, P. Raizada, A. Sudhaik, P. Shandilya, P. Thakur, S. Agarwal, V.K. Gupta, Enhanced photocatalytic activity and stability of AgBr/BiOBr/graphene heterojunction for phenol degradation under visible light, Journal of Saudi Chemical Society 23(5) (2019) 586-599.
[31] Z. Youssef, L. Colombeau, N. Yesmurzayeva, F. Baros, R. Vanderesse, T. Hamieh, J. Toufaily, C. Frochot, T. Roques-Carmes, S. Acherar, Dye-sensitized nanoparticles for heterogeneous photocatalysis:

Cases studies with TiO2, ZnO, fullerene and graphene for water purification, Dyes and Pigments 159 (2018) 49-71.
[32] S. Filice, D. D'Angelo, S. Libertino, I. Nicotera, V. Kosma, V. Privitera, S.J.C. Scalese, Graphene oxide and titania hybrid Nafion membranes for efficient removal of methyl orange dye from water, Carbon 82 (2015) 489-499.
[33] P. Shandilya, D. Mittal, M. Soni, P. Raizada, A. Hosseini-Bandegharaei, A.K. Saini, P. Singh, Fabrication of fluorine doped graphene and SmVO4 based dispersed and adsorptive photocatalyst for abatement of phenolic compounds from water and bacterial disinfection, Journal of Cleaner Production 203 (2018) 386-399.
[34] P. Shandilya, D. Mittal, A. Sudhaik, M. Soni, P. Raizada, A.K. Saini, P. Singh, P. Technology, GdVO4 modified fluorine doped graphene nanosheets as dispersed photocatalyst for mitigation of phenolic compounds in aqueous environment and bacterial disinfection, Separation and Purification Technology 210 (2019) 804-816.
[35] N. Masunga, O.K. Mmelesi, K.K. Kefeni, B.B. Mamba, Recent advances in copper ferrite nanoparticles and nanocomposites synthesis, magnetic properties and application in water treatment, Journal of Environmental Chemical Engineering 7(3) (2019) 103179.
[36] J. Jia, X. Du, Q. Zhang, E. Liu, J. Fan, Z-scheme MgFe2O4/Bi2MoO6 heterojunction photocatalyst with enhanced visible light photocatalytic activity for malachite green removal, Applied Surface Science 492 (2019) 527-539.
[37] S. Taghavi Fardood, F. Moradnia, M. Mostafaei, Z. Afshari, V. Faramarzi, S. Ganjkhanlu, Biosynthesis of MgFe2O4 magnetic nanoparticles and its application in photo-degradation of malachite green dye and kinetic study, Nanochemistry Research 4(1) (2019) 86-93.
[38] A. Ivanets, M. Roshchina, V. Srivastava, V. Prozorovich, T. Dontsova, S. Nahirniak, V. Pankov, A. Hosseini-Bandegharaei, H.N. Tran, M. Sillanpää, Effect of metal ions adsorption on the efficiency of methylene blue degradation onto MgFe2O4 as Fenton-like catalysts, Colloids and Surfaces A: Physicochemical and Engineering Aspects 571 (2019) 17-26.
[39] K. Kirchberg, A. Becker, A. Bloesser, T. Weller, J. Timm, C. Suchomski, R. Marschall, Stabilization of Monodisperse, Phase-Pure MgFe2O4 Nanoparticles in Aqueous and Nonaqueous Media and Their Photocatalytic Behavior, The Journal of Physical Chemistry C 121(48) (2017) 27126-27138.
[40] K. Shetty, B. Prathibha, D. Rangappa, K. Anantharaju, H. Nagaswarupa, H. Nagabhushana, S. Prashantha, Photocatalytic study for fabricated Ag doped and undoped MgFe2O4 nanoparticles, Materials Today: Proceedings 4(11) (2017) 11764-11772.
[41] C.M. Park, Y.M. Kim, K.-H. Kim, D. Wang, C. Su, Y. Yoon, Potential utility of graphene-based nano spinel ferrites as adsorbent and photocatalyst for removing organic/inorganic contaminants from aqueous solutions: A mini review, Chemosphere 221 (2019) 392-402.
[42] P. Singh, P. Shandilya, P. Raizada, A. Sudhaik, A. Rahmani-Sani, A.J.A.J.o.C. Hosseini-Bandegharaei, Review on various strategies for enhancing photocatalytic activity of graphene based nanocomposites for water purification, Arabian Journal of Chemistry 13(1) (2020) 3498-3520.
[43] P. Shandilya, D. Mittal, M. Soni, P. Raizada, J.-H. Lim, D.Y. Jeong, R.P. Dewedi, A.K. Saini, P.J.J.o.t.T.I.o.C.E. Singh, Islanding of EuVO4 on high-dispersed fluorine doped few layered graphene sheets for efficient photocatalytic mineralization of phenolic compounds and bacterial disinfection, Journal of the Taiwan Institute of Chemical Engineers 93 (2018) 528-542.
[44] S. Yang, X. Feng, L. Wang, K. Tang, J. Maier, K. Müllen, Graphene-based nanosheets with a sandwich structure, Angewandte Chemie International Edition 49(28) (2010) 4795-4799.
[45] V. Khot, A. Salunkhe, N. Thorat, R. Ningthoujam, S. Pawar, Induction heating studies of dextran coated MgFe 2 O 4 nanoparticles for magnetic hyperthermia, Dalton Transactions 42(4) (2013) 1249-1258.

[46] W. Zhang, Y. Zheng, X. Zhang, Q. Zhu, L. Tian, H. Wu, H. Yan, S. Qi, Structure-microwave absorption performance correlations of GNPs/ZnO nanocomposite absorber: Synthesis, characteration and mechanism investigation, Ceramics International 45(10) (2019) 13376-13384.
[47] Y. Yin, W. Liu, N. Huo, S. Yang, Synthesis of vesicle-like MgFe2O4/graphene 3D network anode material with enhanced lithium storage performance, ACS Sustainable Chemistry & Engineering 5(1) (2016) 563-570.
[48] B. Rahmanivahid, M. Pinilla-de Dios, M. Haghighi, R. Luque, Mechanochemical Synthesis of CuO/MgAl2O4 and MgFe2O4 Spinels for Vanillin Production from Isoeugenol and Vanillyl Alcohol, Molecules 24(14) (2019) 2597.
[49] T. Yamashita, P. Hayes, Analysis of XPS spectra of Fe2+ and Fe3+ ions in oxide materials, Applied surface science 254(8) (2008) 2441-2449.
[50] A. Mukherjee, S. Chakrabarty, N. Kumari, W.-N. Su, S. Basu, Visible-light-mediated electrocatalytic activity in reduced graphene oxide-supported bismuth ferrite, ACS omega 3(6) (2018) 5946-5957.
[51] W. Yan, X. Cao, K. Ke, J. Tian, C. Jin, R. Yang, One-pot synthesis of monodispersed porous CoFe 2 O 4 nanospheres on graphene as an efficient electrocatalyst for oxygen reduction and evolution reactions, RSC Advances 6(1) (2016) 307-313.
[52] D.D. La, J.M. Patwari, L.A. Jones, F. Antolasic, S.V. Bhosale, Fabrication of a GNP/Fe–Mg binary oxide composite for effective removal of arsenic from aqueous solution, ACS Omega 2(1) (2017) 218-226.
[53] B. Safizade, S. Masoudpanah, M. Hasheminiasari, A. Ghasemi, Photocatalytic activity of BiFeO 3/ZnFe 2 O 4 nanocomposites under visible light irradiation, RSC advances 8(13) (2018) 6988-6995.
[54] Z. Li, Y. Shen, Y. Guan, Y. Hu, Y. Lin, C.-W. Nan, Bandgap engineering and enhanced interface coupling of graphene–BiFeO 3 nanocomposites as efficient photocatalysts under visible light, Journal of Materials Chemistry A 2(6) (2014) 1967-1973.
[55] M. Saravanan, T.S. Girisun, G. Vinitha, Third-order nonlinear optical properties and power limiting behavior of magnesium ferrite under CW laser (532 nm, 50 mW) excitation, Journal of materials science 51(6) (2016) 3289-3296.
[56] N.-u. Ain, W. Shaheen, B. Bashir, N.M. Abdelsalam, M.F. Warsi, M.A. Khan, M. Shahid, Electrical, magnetic and photoelectrochemical activity of rGO/MgFe2O4 nanocomposites under visible light irradiation, Ceramics International 42(10) (2016) 12401-12408.
[57] K. Shetty, S. Lokesh, D. Rangappa, H. Nagaswarupa, H. Nagabhushana, K. Anantharaju, S. Prashantha, Y. Vidya, S.J.P.B.C.M. Sharma, Designing MgFe2O4 decorated on green mediated reduced graphene oxide sheets showing photocatalytic performance and luminescence property, Physica B: Condensed Matter 507 (2017) 67-75.
[58] G.-Q. Qi, C.-L. Liang, R.-Y. Bao, Z.-Y. Liu, W. Yang, B.-H. Xie, M.-B. Yang, s. cells, Polyethylene glycol based shape-stabilized phase change material for thermal energy storage with ultra-low content of graphene oxide, Solar energy materials 123 (2014) 171-177.
[59] D. Ghosh, S. Giri, C.K. Das, Preparation of CTAB-assisted hexagonal platelet Co (OH) 2/graphene hybrid composite as efficient supercapacitor electrode material, ACS Sustainable Chemistry & Engineering 1(9) (2013) 1135-1142.
[60] J. Niu, W.G. Pell, B.E. Conway, Requirements for performance characterization of C double-layer supercapacitors: Applications to a high specific-area C-cloth material, Journal of Power Sources 156(2) (2006) 725-740.
[61] A.G. Tabrizi, N. Arsalani, A. Mohammadi, H. Namazi, L.S. Ghadimi, I. Ahadzadeh, Facile synthesis of a MnFe 2 O 4/rGO nanocomposite for an ultra-stable symmetric supercapacitor, New Journal of Chemistry 41(12) (2017) 4974-4984.
[62] P.M. Shafi, R. Dhanabal, A. Chithambararaj, S. Velmathi, A.C. Bose, α-MnO2/h-MoO3 Hybrid Material for High Performance Supercapacitor Electrode and Photocatalyst, ACS Sustainable Chemistry & Engineering 5(6) (2017) 4757-4770.

[63] H. Wang, Y. Song, X. Ye, H. Wang, W. Liu, L. Yan, Asymmetric Supercapacitors Assembled by Dual Spinel Ferrites@ Graphene Nanocomposites as Electrodes, ACS Applied Energy Materials 1(7) (2018) 3206-3215.
[64] M. Israr, J. Iqbal, A. Arshad, S.O. Aisida, I. Ahmad, A unique ZnFe2O4/graphene nanoplatelets nanocomposite for electrochemical energy storage and efficient visible light driven catalysis for the degradation of organic noxious in wastewater, Journal of Physics and Chemistry of Solids 140 (2020) 109333.
[65] Z. Wang, X. Zhang, Y. Li, Z. Liu, Z. Hao, Synthesis of graphene–NiFe 2 O 4 nanocomposites and their electrochemical capacitive behavior, Journal of Materials Chemistry A 1(21) (2013) 6393-6399.
[66] J. Zhang, J. Jiang, H. Li, X. Zhao, A high-performance asymmetric supercapacitor fabricated with graphene-based electrodes, Energy & Environmental Science 4(10) (2011) 4009-4015.
[67] C. Liu, Z. Yu, D. Neff, A. Zhamu, B.Z. Jang, Graphene-based supercapacitor with an ultrahigh energy density, Nano letters 10(12) (2010) 4863-4868.
[68] Y. Liu, X. Miao, J. Fang, X. Zhang, S. Chen, W. Li, W. Feng, Y. Chen, W. Wang, Y. Zhang, Layered-MnO2 nanosheet grown on nitrogen-doped graphene template as a composite cathode for flexible solid-state asymmetric supercapacitor, ACS applied materials & interfaces 8(8) (2016) 5251-5260.
[69] Y. Chen, J. Zhang, M. Li, C. Yang, L. Zhang, C. Wang, H. Lu, Strong interface coupling and few-crystalline MnO2/Reduced graphene oxide composites for supercapacitors with high cycle stability, Electrochimica Acta 292 (2018) 115-124.
[70] J. Choi, K.-d. Seong, J. Kang, M. Hwang, J.M. Kim, X. Jin, Y. Piao, Fluoride ion-mediated morphology control of fluorine-doped CoFe2O4/graphene sheet composites for hybrid supercapacitors with enhanced performance, Electrochimica Acta 279 (2018) 241-249.
[71] P. Xiong, H. Huang, X. Wang, Design and synthesis of ternary cobalt ferrite/graphene/polyaniline hierarchical nanocomposites for high-performance supercapacitors, Journal of Power Sources 245 (2014) 937-946.
[72] M. Israr, J. Iqbal, A. Arshad, M. Rani, P. Gómez-Romero, R. Benages, Graphene triggered enhancement in visible-light active photocatalysis as well as in energy storage capacity of (CFO) 1-x (GNPs) x nanocomposites, Ceramics International 46(3) (2020) 2630-2639.
[73] T. Zhou, G. Zhang, P. Ma, X. Qiu, H. Zhang, H. Yang, G.J.J.o.A. Liu, Compounds, Efficient degradation of rhodamine B with magnetically separable Ag3PO4@ MgFe2O4 composites under visible irradiation, Journal of Alloys and Compounds 735 (2018) 1277-1290.
[74] J. Chen, D. Zhao, Z. Diao, M. Wang, L. Guo, S. Shen, interfaces, Bifunctional modification of graphitic carbon nitride with MgFe2O4 for enhanced photocatalytic hydrogen generation, ACS applied materials & interfaces 7(33) (2015) 18843-18848.
[75] P. Singh, S. Gautam, P. Shandilya, B. Priya, V.P. Singh, P. Raizada, Graphene bentonite supported ZnFe2O4 as superparamagnetic photocatalyst for antibiotic degradation, Adv. Mater. Lett. 8(3) (2017) 229-238.
[76] F. Wang, X. Yu, M. Ge, S. Wu, One-step synthesis of TiO2/γ-Fe2O3/GO nanocomposites for visible light-driven degradation of ciprofloxacin, Chemical Engineering Journal 384 (2020) 123381.
[77] P.V. Kamat, Graphene-based nanoassemblies for energy conversion, The Journal of Physical Chemistry Letters 2(3) (2011) 242-251.
[78] Q. Liu, Z. Liu, X. Zhang, L. Yang, N. Zhang, G. Pan, S. Yin, Y. Chen, J. Wei, Polymer photovoltaic cells based on solution-processable graphene and P3HT, Advanced Functional Materials 19(6) (2009) 894-904.
[79] A. Kumar, P. Raizada, P. Singh, R. Saini, A. Saini, A. Hosseini-Bandegharaei, Perspective and status of polymeric graphitic carbon nitride based Z-scheme photocatalytic systems for sustainable photocatalytic water purification, Chemical Engineering Journal 391 (2019) 123496.

[80] X. Wang, L. Zhi, K.J.N.l. Müllen, Transparent, conductive graphene electrodes for dye-sensitized solar cells, Nano letters 8(1) (2008) 323-327.
[81] F. Wang, X. Yu, M. Ge, S. Wu, J. Guan, J. Tang, X. Wu, R.O. Ritchie, Facile self-assembly synthesis of γ-Fe2O3/graphene oxide for enhanced photo-Fenton reaction, Environmental Pollution 248 (2019) 229-237.
[82] F. Wu, W. Duan, M. Li, H. Xu, Synthesis of MgFe2O4/Reduced Graphene Oxide Composite and Its Visible-Light Photocatalytic Performance for Organic Pollution, International Journal of Photoenergy 2018 (2018).
[83] S.J. Uke, S.P. Mardikar, D.R. Bambole, Y. Kumar, G.N. Chaudhari, Sol-gel citrate synthesized Zn doped MgFe2O4 nanocrystals: A promising supercapacitor electrode material, Materials Science for Energy Technologies 3 (2020) 446-455.
[84] L. Luo, Z. Chen, H. Ke, S. Sha, G. Cai, D. Li, H. Yang, X. Yang, R. Zhang, J.J.M. Li, Design, Facile synthesis of three-dimensional MgFe2O4/graphene aerogel composites for high lithium storage performance and its application in full cell, Materials & Design 182 (2019) 108043.
[85] Y. Yin, W. Liu, N. Huo, S.J.A.S.C. Yang, Engineering, Synthesis of vesicle-like MgFe2O4/graphene 3D network anode material with enhanced lithium storage performance, ACS Sustainable Chemistry & Engineering 5(1) (2017) 563-570.

List of Figures